Pure Appl. Geophys. 175 (2018), 2279–2291

https://doi.org/10.1007/s00024-018-1777-1

Pure and Applied Geophysics

A Winter Precipitation Reconstruction (CE 1810–2012) in the Southeastern Tibetan Plateau and Its Relationship to Salween River Streamflow Variations

Feng Chen,[1] Yujiang Yuan,[1] Zexin Fan,[2] and Shulong Yu[1]

Abstract—We established a tree-ring width series from one Yunnan Douglas fir (*Pseudotsuga forrestii*) stand near the Mingyong glacier terminus of Meili Snow Mountain, southeastern Tibetan Plateau. Correlation analyses indicated that radial growth of Yunnan Douglas firs is largely controlled by variations in winter (November–March) precipitation. The precipitation reconstruction model accounts for 37% of the actual precipitation variance during the common period 1954–2012. Spatial correlations with the gridded precipitation data reveal that the winter precipitation reconstruction represents regional precipitation changes over the southeastern Tibetan Plateau. By comparing our results with other regional tree-ring records, a distinctive amount of common dry and humid periods were found. Our winter precipitation reconstruction shows profound similarities with Salween river streamflow signals as well as regional glacial activity. Cross-wavelet analysis reveals solar and ENSO influences on precipitation and streamflow variations in the southeastern Tibetan Plateau.

Key words: Tree rings, southeastern Tibetan Plateau, Salween River, winter precipitation reconstruction, ENSO.

1. Introduction

Due to the economic development and rapidly growing human populations in Asia, water resource demands for agricultural production, drinking water and hydropower generation are increasing at a rapid pace. In addition, the recent acceleration in climate warming has had a significant influence on the hydrological variations and ecosystems of the Asian monsoon regions, and has repeatedly affected the livelihood of billions of people (Cook et al. 2010; Dai 2011; Bae et al. 2015). As the youngest and the highest plateau in Asia, the Tibetan Plateau (TP) is still undergoing structural changes, and is the abode of glaciers and snowpack (Bräuning 2006; Yang et al. 2016; Pratap et al. 2016). Since it is the source of the main Asian rivers, hydroclimatic variation in the TP plays a vital role in the supply of fresh water for the adjacent countries of southern and southeastern Asia, and can have wide-ranging geopolitical consequences (He and Liu 2001; Vinke et al. 2016). The recent glacial retreat in the TP with climate warming raises further concern regarding adequate supply to meet the huge demand for fresh water (Yao et al. 2004; Kulkarni and Karyakarte 2014; Fang et al. 2016). Over the past 60 years, the spatiotemporal coverage of observational hydroclimatic records in the TP has been improved, and many hydroclimatic characteristics of the TP have been revealed (Xu et al. 2008). However, because of instrumental sensitivity and collection efficiency of snow crystals, the measurement of solid precipitation during winter is always difficult (Gultepe et al. 2017), especially in the TP. This limits the analysis of long-term hydroclimatic trends from instrumental climate records and requires the study of hydroclimatic history from high-resolution proxy data.

Tree rings can greatly enhance our understanding of past hydroclimatic variability in the Asian monsoon regions (Cook et al. 2010). Several tree-ring chronologies have been developed from the southeastern TP in recent years that capture regional and large-scale hydroclimatic variation (Bräuning and Mantwill 2004; Fan et al. 2008a, 2010; Gou et al. 2013; Liu et al. 2014; Zhang et al. 2015; Grießinger

[1] Key Laboratory of Tree-Ring Physical and Chemic Research of China Meteorological Administration, Key Laboratory of Tree-Ring Ecology of Uigur Autonomous Region, Institute of Desert Meteorology, China Meteorological Administration, No 46 Jianguo Road, Ürümqi, China. E-mail: feng653@163.com
[2] Key Laboratory of Tropical Forest Ecology, Xishuangbanna Tropical Botanical Garden, Chinese Academy of Sciences, 88 Xuefu Road, Kunming, China.

et al. 2016). These hydroclimatic reconstructions enable us to describe the long-term hydroclimatic history across the southeastern TP. However, hydroclimatic reconstructions from the Asian river gorges of the Mekong, Yangtze and Salween in Yunnan province (China) are still underrepresented. Despite the availability of coniferous forests, no precipitation reconstructions have been developed from the Salween River (Nu River) Basin in the southeastern TP.

In this work, we present a tree-ring-based winter precipitation reconstruction (1810–2012) from the southeastern TP. We analyze the temporal characteristics of the precipitation reconstruction and put recent precipitation variations into a long-term context. Based on this reconstruction, we also analyze the intensity, frequency and duration of drought and pluvial events, and examine the associations with the observed streamflow of Salween River. Finally, to identify the major forces affecting the variation in precipitation, we compare the precipitation reconstruction with the sunspot number series and El Niño-Southern Oscillation (ENSO) index (Li et al. 2011).

2. Materials and Methods

2.1. Regional Setting and Tree-Ring Data

The sampling site is located in the Hengduan Mountain range, southeastern TP (Fig. 1). Many Asian rivers flow through the study area, including the Yangtze, Salween, Mekong and Irrawaddy. With high biodiversity value, the region is covered in widespread forests. The study areas are influenced by the Indian summer monsoon. The monsoonal air masses flowing over the Bay of Bengal bring plenty of rainfall for this area during the summer months, whereas continental air masses (Asian winter monsoon) dominate and lead to dry and cold conditions in winter (Li et al. 2015). According to the data from climate stations in Deqin, the annual temperature is 5.5 °C, with a mean temperature of − 2.3 °C in January and 12.6 °C in July. Total annual precipitation is 644 mm, with precipitation during the warm season (June to September) accounting for 59% of the total (Fig. 2a). The mean annual temperature showed a significant upward trend from the 1980s, and no significant upward trends were found in the annual precipitation (Fig. 2b).

The tree-ring cores were collected near the Mingyong glacier of Meili Snow Mountain (28°28′N, 98°46′E, 2900 m a.s.l.) in May 2013 (Table 1). The sampling site is covered by mixed coniferous broad-leaved forest including sparse Yunnan Douglas fir (*Pseudotsuga forrestii*) of 40–50 m height, growing on relatively thin soil. Forty cores were sampled from 23 living trees using an increment borer. After standard surface preparation, each annual ring was measured with a TA UniSlide Measurement System. The COFECHA software program (Holmes 1983) was applied to control the quality of cross-dating. The average rate of absent rings in the samples was 0.53%.

To remove non-climatic trends, cross-dated tree-ring width series were detrended with a negative exponential curve or 80-year cubic smoothing spline. The ARSTAN program was applied to produce a site chronology from the detrended tree-ring width series (Cook 1985). We used residual chronology, which captures the high-frequency common variance in this study. The expressed population signal (EPS) and inter-series correlation (Rbar) were used to verify the replicated chronological period (Wigley et al. 1984). Both EPS and Rbar were computed over 50 years, lagged by 25 years.

2.2. Climate Data and Statistical Analysis

Instrumental climate records for Deqin (28°27′N, 98°53′E, 3488 m a.s.l.), including monthly mean temperatures and total precipitation, were compared to the residual chronology. The climate data cover the period from August 1953 to December 2014. We also used gridded precipitation data (0.5° × 0.5°) for the climate response analyses. This gridded monthly climate data was downloaded from the Climatic Research Unit (CRU), East Anglia, UK, for our research area for 1953–2014 (averaged over 28–29°N, 98–99°E). Tree-ring/climate relationships were tested for both meteorological and gridded datasets from the previous June to the current September.

We used a split calibration-verification scheme to evaluate the stability of the model (Cook and

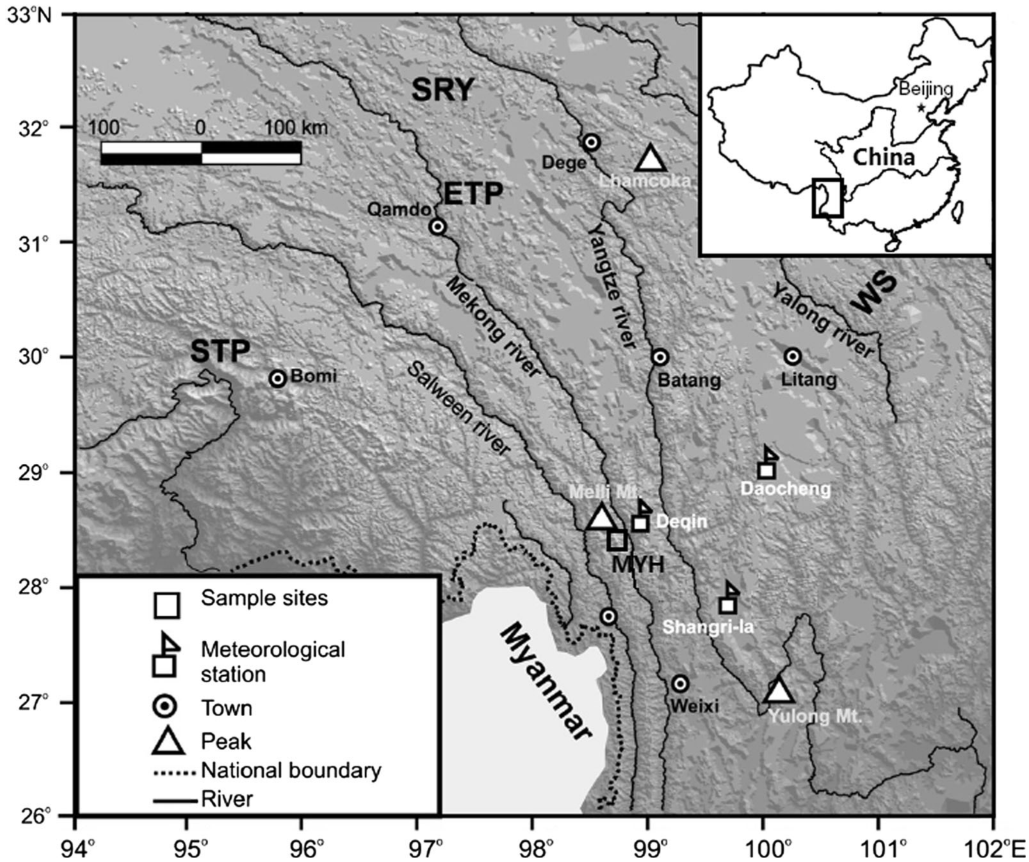

Figure 1
Location map of sampling site (MYH) and surrounding meteorological stations

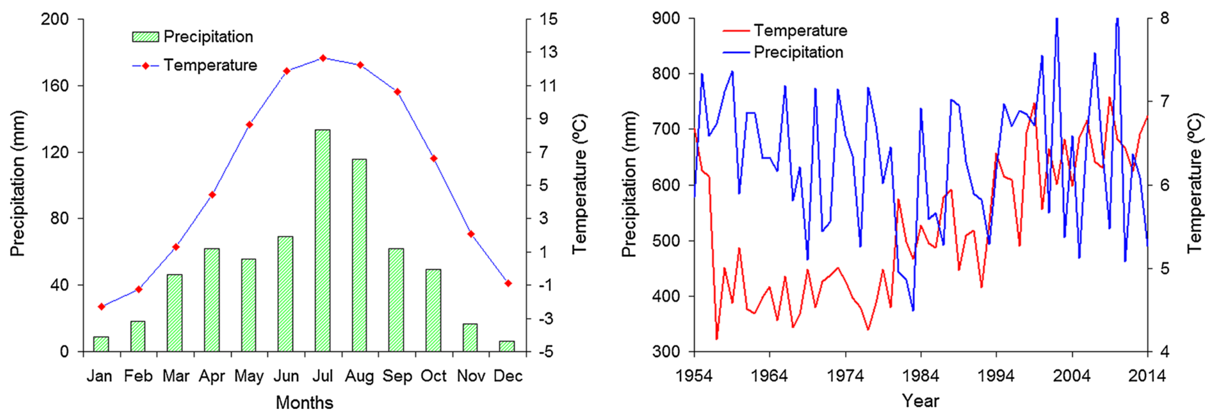

Figure 2
Total monthly precipitation and monthly mean temperature records at the Deqin meteorological station. Comparison between observed annual precipitation and temperature during the period 1954–2014

Table 1

Tree-ring site and the corresponding meteorological and hydrological station in the Salween River Basin

Site	Lat. (N)	Long. (E)	Elevation (m)	Aspect	Slope	Cores/trees	Species	Period
MYH	28°28′	98°46′	2900	SE	20–30°	40/23	*Pseudotsuga forrestii*	1810–2012
Deqin	28°27′	98°53′	3488					1953–2014
Daojieba	24°59′	98°53′	685					1960–2009

See Fig. 1 for locations

Kairiukstis 1990). There are 59 years of precipitation data during the common period 1954–2012. The period from 1954 to 1982 was used for verification and 1983–2012 for calibration; this process was then reversed. The test values used included the sign test, the reduction of error (RE) and coefficient of efficiency (CE). Furthermore, considering the long-term memory and the distribution of precipitation (Efstathiou and Varotsos 2012), wavelet analysis was used to investigate how the periodicities of the reconstructions may change through time (Torrence and Compo 1998). In addition, the KNMI Climate Explorer (http://www.knmi.nl) was applied to investigate the spatial correlation between sea surface temperature (SST, Rayner et al. 2003) and our precipitation reconstruction. Furthermore, in order to investigate the association between extreme events during the instrumental period and the circulation patterns, composites of 500 hPa vector wind anomalies (January to March) were created using NCEP reanalysis data (Kalnay et al. 1996) for the wettest and driest years ($n = 10$).

3. Results

3.1. Precipitation Reconstruction

Based on the EPS threshold (0.85), the residual chronology met an acceptable signal strength after CE 1810 (sample depth $\geq$ 5 individuals). The residual chronology has relatively low year-to-year variation (mean sensitivity = 0.268), which is typical for trees growing in relatively moist habitats. Comparable high inter-series correlations (Rbar = 0.42–0.69) indicated that the residual chronology contains strong common signals. The residual chronology shows significant ($p < 0.01$) positive correlations with precipitation (station and gridded) in the previous November and current March (Fig. 3). However, with the exception of the gridded temperature for the current July ($r = 0.35$), there were no significant correlations between the residual chronology and temperature. The highest correlation ($r = 0.61$, $P < 0.001$) was found between the gridded winter (November–March) precipitation and the residual chronology. Therefore, we used winter precipitation as a target for our reconstruction. As shown in Table 2, the verification and calibration results indicated a good model fit (Table 2). The reconstruction model explained 37% of the total November–March precipitation variance during the common period 1954–2012 (Fig. 4).

3.2. Characteristics of the Winter Precipitation Reconstruction

The winter precipitation reconstruction for the southeastern TP is presented in Fig. 5a. The average winter precipitation is estimated at 75.7 mm, and the standard deviation (σ) is 17.4, for the period CE 1810–2012. Dry and wet periods were determined if the 10-year low-pass-filtered values were lower (or higher) than the long-term mean for a continuous period of more than 10 years. Dry periods occurred in CE 1829–1842, 1857–1876, 1922–1934, 1958–1970, 1978–1988 and 2002–2012, whereas wet periods were identified for CE 1817–1828, 1843–1856, 1948–1957 and 1989–2001. Notably, a downward trend was found in our precipitation reconstruction during the period 1990–2012.

The spatial correlation analysis indicates that high positive correlation fields were found in the southeastern TP, and revealed that this precipitation

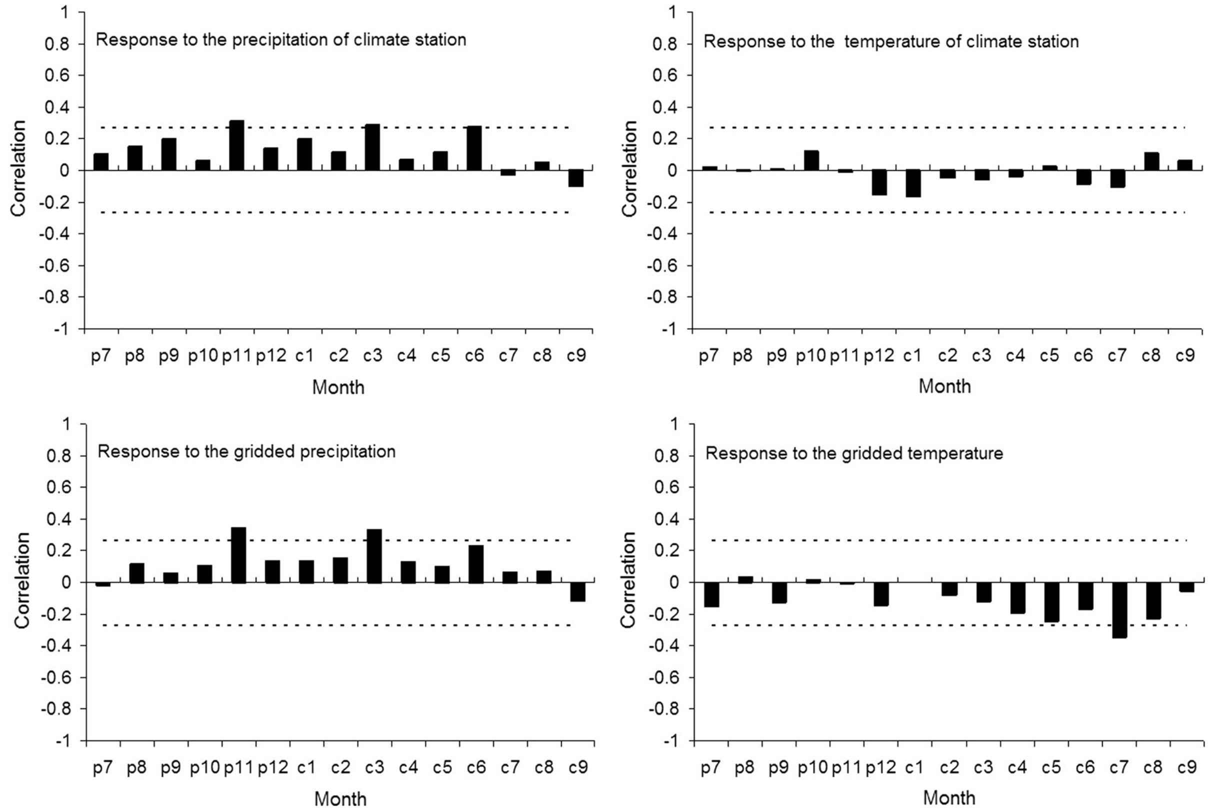

Figure 3
Response plots for the residual chronology with total monthly precipitation and mean monthly temperature over the period 1954–2012. Coefficients were calculated from the previous July to the current September. Dotted lines indicate level of significance at $p < 0.05$

Table 2

Statistical calibration and verification test results for the common period CE 1954–2012

	Calibration (1983–2012)	Verification (1954–1982)	Calibration (1954–1983)	Verification (1983–2012)	Full calibration (1954–2012)
r	0.55	0.66	0.66	0.55	0.61
r^2	0.30	0.44	0.44	0.30	0.37
RE		0.42		0.28	
CE		0.32		0.16	
Sign test		22+/7−[b]		21+/8−[a]	

[a]Significance at $p < 0.05$

[b]Significance at $p < 0.01$

reconstruction represents broad-scale regional winter precipitation changes (Fig. 6a). Temporal features of the cycles in our precipitation reconstruction were show in Fig. 6b. The wavelet indicates significant power at 8–11 years for three periods centered in 1810, 1880 and 1950. Significant (though less robust) power at 25–30 years is detected in the periods 1810–1820 and 1990–2010.

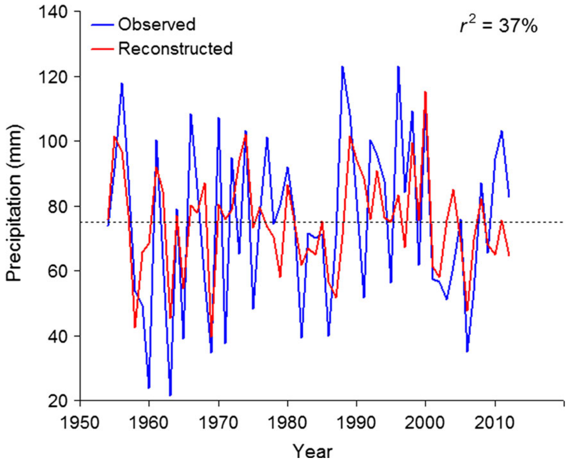

Figure 4
Comparison between observed and reconstructed winter precipitation for the southeastern Tibetan Plateau from 1954 to 2012

4. Discussion

4.1. Impacts of Winter Precipitation Changes on Glacial Mass and Runoff

Retreat and advance phases of monsoonal glaciers in the southeastern TP are largely influenced by changes in warm season temperature (Shi 2002; Bräuning 2006). In particular, variations in precipitation have a significant effect on glacial mass balance in the southeastern TP (Yang et al. 2016). The precipitation in winter falls as snow, and nourishes the glaciers (Seko and Takahashi 1991; Nesje 2005; Gultepe et al. 2017). However, winter precipitation is hard to measure accurately, especially at high altitudes. The winter precipitation reconstruction based on tree-ring data provides some solid precipitation information for us. A comparison of our winter precipitation reconstruction with mean annual temperature reconstruction (Fan et al. 2008b) and

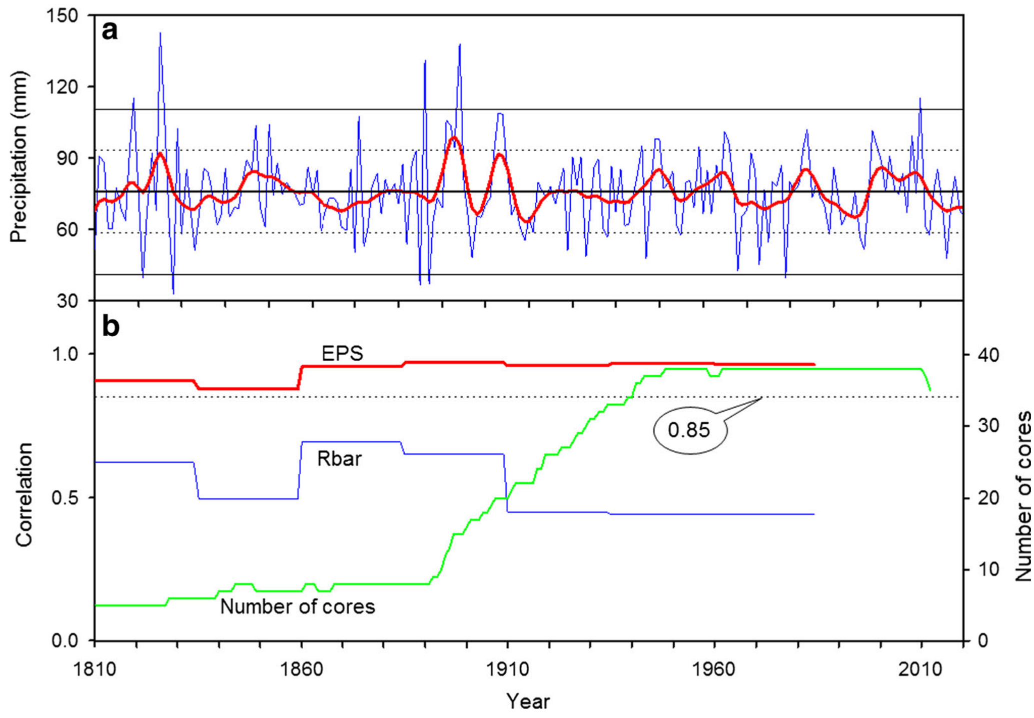

Figure 5
a Reconstructed total November–March precipitation for the southeastern Tibetan Plateau. The bold line was smoothed with a 10-year FFT (fast Fourier transform) filter. The central horizontal line shows the mean of the estimated values; inner horizontal (dotted) lines show the border of one standard deviation, and outer horizontal lines show two standard deviations. The date AD 1810 indicates that, based on the EPS cut-off of 0.85, the chronology (sample depth > 5 individuals) is reliable after that date. **b** Plot of the running expressed population signal (EPS) and the running series of average correlation (Rbar)

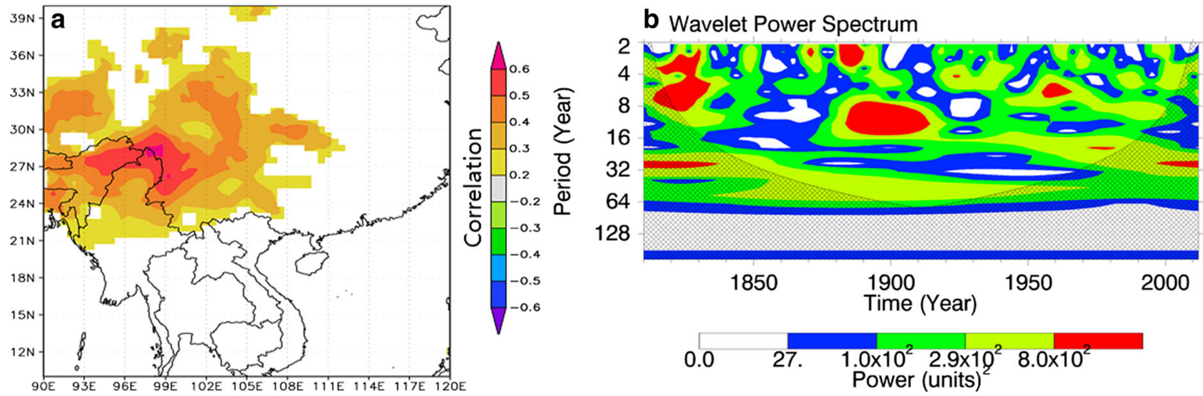

Figure 6
a Spatial correlation fields of reconstructed winter precipitation for southeastern Tibetan Plateau with regional gridded winter precipitation for the period 1954–2012. **b** The wavelet power spectrum. The color contour intervals represent 75, 50, 25 and 5% of the wavelet power, respectively

Mingyong glacier fluctuation (Zheng et al. 1999) reveals a cold-wet (strong) 1900s (glacier advance), warm-wet (strong) 1940–1950s (glacier retreat), cold-wet (strong) 1970s (glacier advance), warm-wet (strong) 1990s (glacier advance) and warm-dry (strong) 2000s (glacier retreat). During significant wet periods when snow increases in the mountainous areas, increased snow accumulation causes glacier advance. During significant warm periods, decreased snow accumulation causes glacier retreat.

Studies have revealed that snow precipitation plays some important role in the hydrological cycle (Jorg-Hess et al. 2015; Gultepe et al. 2017). Thus, positive correlations are found between our winter precipitation reconstruction and the March–May streamflow of Salween River (Daojieba hydrological station, 98°53′E,24°59′N,685 m a.s.l.), computed over the 1960–2009 common period, with $r = 0.55$ (Fig. 7), increasing to 0.70 after 9-year smoothing. Although the winter precipitation is not as impressive in intensity as the summer precipitation, and accounts for only 15% of annual precipitation, it is of vital importance in generating the seasonal streamflow of Salween River. Thus, to a certain extent, this winter precipitation reconstruction is also representative of the spring streamflow of Salween River. The downward trend in precipitation during the period 1990–2010s with glacial retreat would significantly influence the hydrological cycle and regional ecological systems (Baker and Moseley 2007).

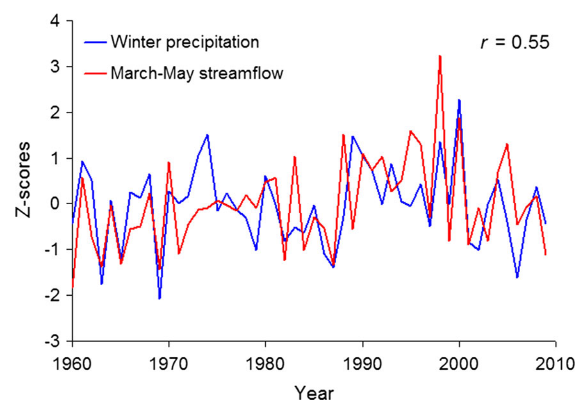

Figure 7
Comparison between reconstructed winter precipitation for southeastern Tibetan Plateau and March–May streamflow of Salween River from 1960 to 2009

4.2. *Comparison with Other Drought Reconstructions*

Some studies revealed that the tree growth in the southeastern TP is significantly influenced by the occurrences of droughts in winter and spring (Fan et al. 2008b; Gou et al. 2013). Some precipitation/drought reconstructions have been presented from the surrounding areas based on tree-ring data (Fan et al. 2008b; Fang et al. 2010; Gou et al. 2013). Despite differences in site locations and tree species, there is a statistically reasonable relationship ($r = 0.35$, $n = 197$, $p < 0.001$) between our precipitation reconstruction and the precipitation-sensitive tree-ring chronology (Gou et al. 2013) which together cover the Great river gorges region in Yunnan. The comparison also revealed that dry conditions during CE 1810s, 1863–1889, 1908–1920, 1928–1936, 1957–1963, 1968–1972, 1982–1989 and 2006–2012, and wet conditions during CE 1822–1828, 1843–1853, 1889–1907, 1938–1943 and 1990–2002 were found in the southeastern TP (Fig. 8). The dry periods CE 1810s, 1835–1844, 1860–1876, 1885–1889, 1907–1923, 1944–1948, 1959–1962, 1967–1973, 1979–1989 and 2006–2012, and the wet periods CE 1824–1827, 1891–1905, 1939–1943, 1949–1958, 1972–1977 and 1999–2005 were found in the neighboring area (Fang et al. 2010). Some differences (i.e. 1830s, 1920s, 1960s) may reflect the complex mountain terrain of southeastern TP and spatial differences in drought variation.

4.3. Precipitation (Streamflow) and Circulation Analysis

ENSO activity is closely linked with large-scale atmospheric circulations of the Asia–Pacific region, which in turn affect drought variations over much of China (Zhang et al. 1999; Li et al. 2011). To establish the relationship between precipitation changes of the southeastern TP and ENSO, we analyzed the correlation between our winter precipitation reconstruction and the reconstructed January–March ENSO index (Li et al. 2011) for the period 1810–2002. We found significant correlation ($r = -0.21$, $p < 0.01$) between our winter precipitation reconstruction and the ENSO index. The cross-wavelet transform of our winter precipitation and the ENSO index is shown in Fig. 9a. There exists a significant negative relationship ($p < 0.01$) in the 2–8-year band from the period 1810–2002. The arrows show the anti-phase

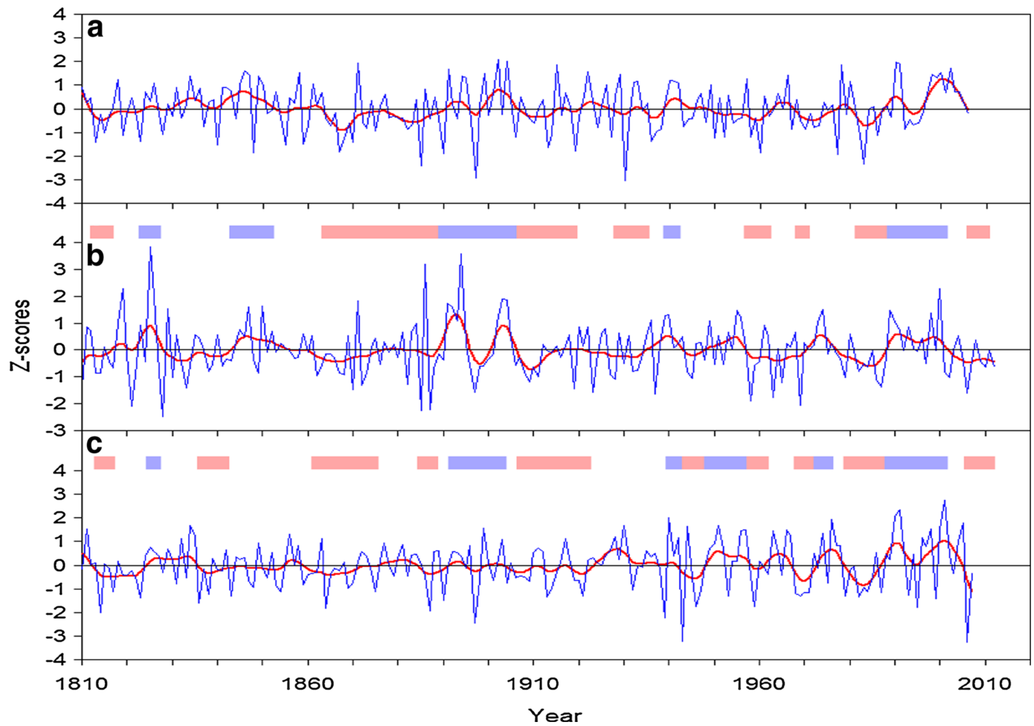

Figure 8

Comparison between the reconstructed precipitation and other moisture-sensitive tree-ring width series. **a** A precipitation-sensitive tree-ring width series from southwestern Sichuan Province (Gou et al. 2013). **b** Reconstructed winter precipitation for southeastern Tibetan Plateau (this study). **c** A moisture-sensitive tree-ring width series from the southeastern Tibetan Plateau (Fang et al. 2010). All series were adjusted for their long-term means over the period 1810–2012, and smoothed with a 10-year low-pass filter to emphasize long-term fluctuations. Red shading represents dry periods; blue shading represents wet periods

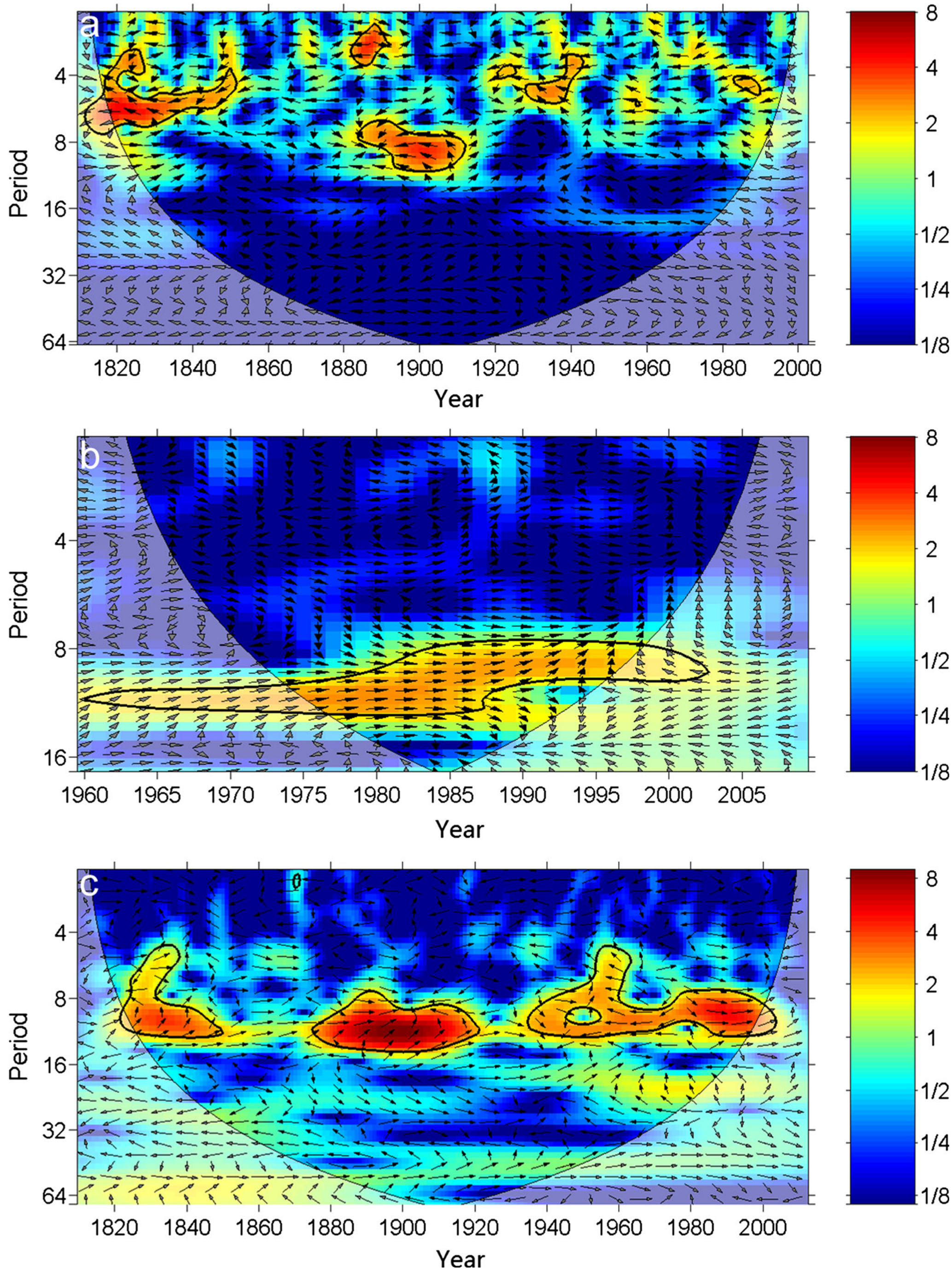

Figure 9

a Cross-wavelet transform between the reconstructed precipitation and ENSO index (Li et al. 2011). **b** Cross-wavelet transform between the March–May streamflow of Salween River and sunspot number series. **c** Cross-wavelet transform of the reconstructed precipitation and sunspot number series. The 5% significance level against red noise is shown as a thick contour. The relative phase relationship is shown as arrows (with in-phase pointing right, anti-phase pointing left)

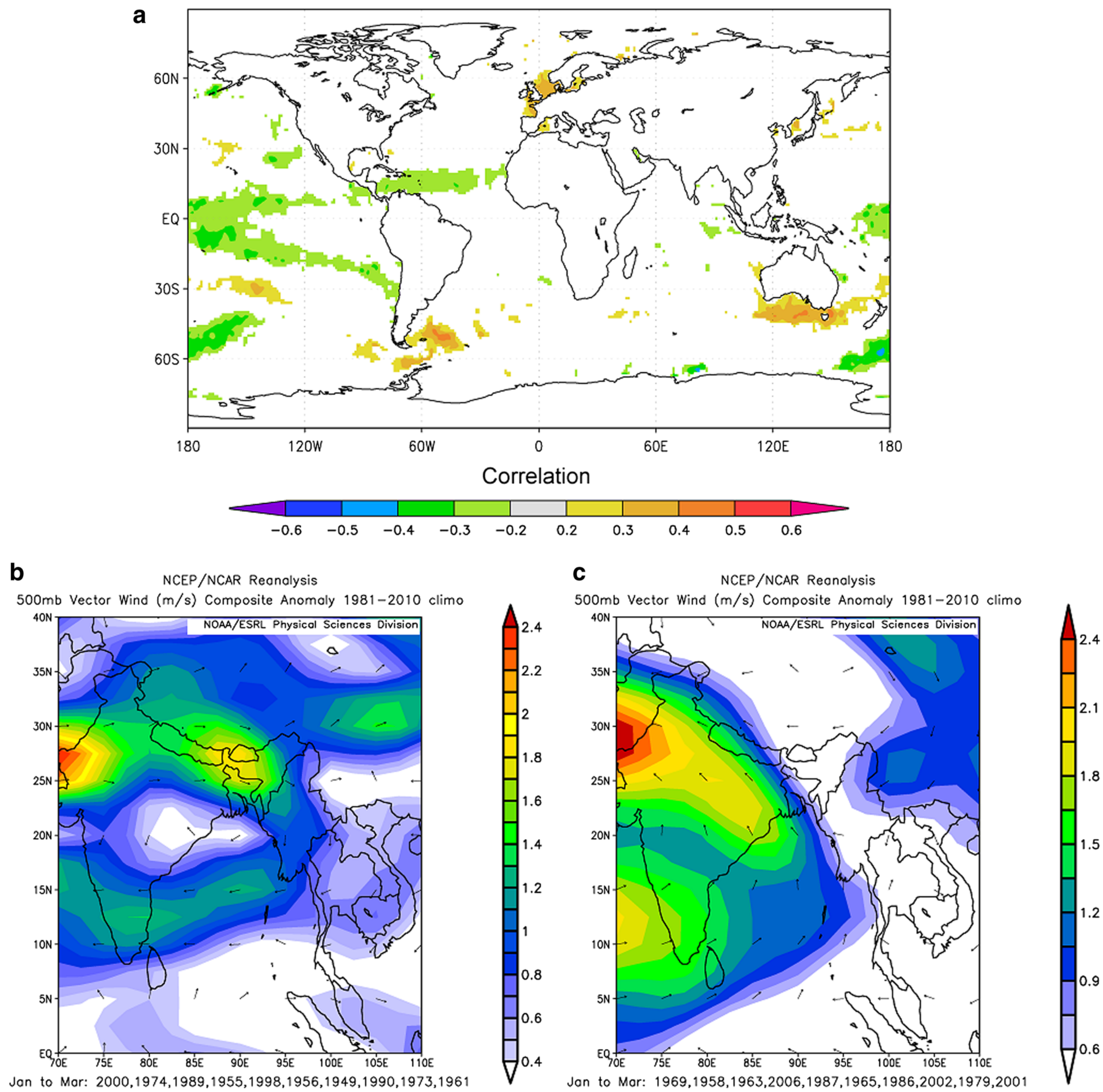

Figure 10

Correlation patterns of the reconstructed rainfall (**a**) with the gridded SST data set of HadISST1 (Rayner et al. 2003) over their overlapping periods from 1950 to 2012. Composite anomaly maps of 500-hPa vector wind (January–March) for the 10 wet (**b**) and 10 dry (**c**) years for precipitation reconstruction during the period 1948–2010

relationships ($p < 0.01$) during the periods 1810–1850s, 1880–1920, 1940–1950s and 1990–2000s. Significant negative correlations between our winter precipitation reconstruction and SSTs are also found in the eastern tropical Pacific Ocean, suggesting possible tele-connections between the winter precipitation of the southeastern TP and the climate variability of the Pacific Ocean (Fig. 10a). The 500-hPa vector wind composite anomalies of the wettest years reveal that mean 500-hPa winds exhibit strong westerly and south-westerly flow over southern Asia and the southeastern TP (Fig. 10b). This is consistent with the strong southwesterly wet flow from southern Asia and the

Bay of Bengal, which should bring sufficient water vapor to form snow. During the driest years, the opposite pattern occurs (Fig. 10c). As shown above, precipitation conditions in the southeastern TP are related to various parts of remote oceans.

A number of studies have revealed that solar activity can influence streamflow changes in direct and indirect ways (Zanchettin et al. 2008; Prokoph et al. 2012; Fu et al. 2012). The relationship between the March–May streamflow of Salween River and sunspot number was examined, and the potential effects of solar activity on Salween River streamflow changes were discussed. A comparison of the March–May streamflow of Salween River with the sunspot number series reveals no systematic relationship on annual to interannual scales, likely related to the strong interannual streamflow variability. Detailed analysis, however, reveals the existence of a significant in-phase relationship in the 8–11-year band from the 1960 to the 2000s (Fig. 9b). As mentioned above, our winter precipitation reconstruction also recorded the streamflow signals. Thus, the relationship between our winter precipitation reconstruction and the number of sunspots was also examined. A comparison over the past 203 years with the sunspot number series indicates some low-frequency coherency with our precipitation record, and the arrows show an in-phase relationship from the 1820–1840s, 1870–1920s, 1940–1950s and 1980–2010s on a time scale of quasi-11 years (Fig. 9c). Based on the instrumental records, negative correlations were found between the sunspot number series and SSTs in the eastern Pacific Ocean (Roy and Haigh 2010). The cold phases of ENSO (La Niña) have often coincided with the peak annual sunspot number years of the solar cycles (Roy and Haigh 2010). During these cold phases, more precipitation occurs in the southeastern TP, resulting in increased Salween River streamflow. However, the influence of solar activity on streamflow is more complicated than anticipated, and an anti-phase relationship was found during the period 1960–1970s on a time scale of quasi-11 years. Further studies are needed to better understand the relationship among precipitation, streamflow and solar activity.

5. Conclusions

We constructed a tree-ring width series based on samples of Yunnan Douglas firs growing near the Mingyong glacier of Meili Snow Mountain, southeastern TP. A significant positive link was revealed between tree-ring chronology and winter precipitation. Winter precipitation in the southeastern TP was reconstructed based on tree-ring width data over the past 203 years. This reconstruction represents regional winter precipitation variations in the southeastern TP. These findings also indicate that this reconstruction is an appropriate record of Salween River streamflow variation, and is closely linked to glacial activity. A comparison with other precipitation-sensitive tree-ring width series shows high coherency at the decadal scale across the southeastern TP. In addition, cross-wavelet analysis reveals some correlations among the precipitation and streamflow of the southeastern TP and ENSO. This research enhances our understanding of the relationship between the precipitation and streamflow of the southeastern TP and ENSO beyond the relatively short instrumental period.

Acknowledgements

This work was supported by the NSFC (91547115 and 41405081). We thank the reviewers very much whose comments greatly benefitted this manuscript. The precipitation reconstruction is available at the NOAA Paleoclimatology website (https://www.ncdc.noaa.gov/cdo-web/).

References

Bae, D. H., Koike, T., Awan, J. A., Lee, M. H., & Sohn, K. H. (2015). Climate change impact assessment on water resources and susceptible zones identification in the Asian monsoon region. *Water Resources Research, 29*(14), 5377–5393.

Baker, B. B., & Moseley, R. K. (2007). Advancing treeline and retreating glaciers: Implications for conservation in Yunnan, PR China. *Arctic, Antarctic, and Alpine Research, 39*(2), 200–209.

Bräuning, A. (2006). Tree-ring evidence of 'Little Ice Age' glacier advances in southern Tibet. *The Holocene, 16*(3), 369–380.

Bräuning, A., & Mantwill, B. (2004). Summer temperature and summer monsoon history on the Tibetan plateau during the last

400 years recorded by tree rings. *Geophysical Research Letters, 31,* L24205. https://doi.org/10.1029/2004-GL020793.

Cook, E. R. (1985). *A time series analysis approach to tree-ring standardization*. Ph.D. thesis, University of Arizona, Tucson

Cook, E. R., & Kairiukstis, L. A. (1990). *Methods of Dendrochronology*. Dordrecht: Kluwer Academic Press.

Cook, E. R., Anchukaitis, K. J., Buckley, B. M., D'Arrigo, R. D., Jacoby, G. C., & Wright, W. E. (2010). Asian monsoon failure and megadrought during the last millennium. *Science, 328*(5977), 486–489.

Dai, A. (2011). Drought under global warming: A review. *Wiley Interdisciplinary Reviews: Climate Change, 2*(1), 45–65.

Efstathiou, M. N., & Varotsos, C. A. (2012). Intrinsic properties of Sahel precipitation anomalies and rainfall. *Theoretical and Applied Climatology, 109*(3–4), 627–633.

Fan, Z. X., Bräuning, A., & Cao, K. F. (2008a). Tree-ring based drought reconstruction in the central Hengduan Mountains (China) since A.D. 1655. *International Journal of Climatology, 28,* 1879–1887.

Fan, Z. X., Bräuning, A., & Cao, K. F. (2008b). Annual temperature reconstruction in the central Hengduan Mountains, China, as deduced from tree rings. *Dendrochronologia, 26*(2), 97–107.

Fang, Y., Cheng, W., Zhang, Y., Wang, N., Zhao, S., Zhou, C., et al. (2016). Changes in inland lakes on the Tibetan Plateau over the past 40 years. *Journal of Geographical Sciences, 26*(4), 415–438.

Fang, K., Gou, X., Chen, F., Li, J., D'Arrigo, R., Cook, E., et al. (2010). Reconstructed droughts for the southeastern Tibetan Plateau over the past 568 years and its linkages to the Pacific and Atlantic Ocean climate variability. *Climate Dynamics, 35*(4), 577–585.

Fu, C., James, A. L., & Wachowiak, M. P. (2012). Analyzing the combined influence of solar activity and El Niño on streamflow across southern Canada. *Water Resources Research, 48,* W05507. https://doi.org/10.1029/2011WR011507.

Gou, X., Yang, T., Gao, L., Deng, Y., Yang, M., & Chen, F. (2013). A 457-year reconstruction of precipitation in the southeastern Qinghai-Tibet Plateau, China using tree-ring records. *Chinese Science Bulletin, 58*(10), 1107–1114.

Grießinger, J., Bräuning, A., Helle, G., Hochreuther, P., & Schleser, G. (2016). Late Holocene relative humidity history on the southeastern Tibetan plateau inferred from a tree-ring δ^{18}O record: Recent decrease and conditions during the last 1500 years. *Quaternary International*. https://doi.org/10.1016/j.quaint.2016.02.011.

Gultepe, I., Heymsfield, A. J., Field, P. R., & Axisa, D. (2017). Ice-phase precipitation. *AMS Meteorological Monographs, 58*, 6.1–6.36. https://doi.org/10.1175/amsmonographs-d-16-0013.1.

He, D. M., & Liu, X. J. (2001). Equitable utilisation and effective protection of sharing transboundary water resources: International rivers of western China. *Journal of Geographical Sciences, 11*(4), 490–500.

Holmes, R. L. (1983). Computer-assisted quality control in tree-ring dating and measurement. *Tree-Ring Bulletin, 44,* 69–75.

Jorg-Hess, S., Griessinger, N., & Zappa, M. (2015). Probabilistic forecasts of snow water equivalent and runoff in mountainous areas. *Journal of Hydrometeorology, 16,* 2169–2186.

Kalnay, E., Kanarmitsu, M., Kistler, R., Collins, W., Deaven, D., Gandin, L., et al. (1996). The NCEP/NCAR reanalysis 40-year project. *Bulletin of the American Meteorological Society*, *77*(3), 437–471.

Kulkarni, A. V., & Karyakarte, Y. (2014). Observed changes in Himalayan glaciers. *Current Science, 106*(2), 237–244.

Li, J., Xie, S.-P., Cook, E. R., Huang, G., D'Arrigo, R., Liu, F., et al. (2011). Interdecadal modulation of El Niño amplitude during the past millennium. *Nature Climate Change*, *1*(2), 114–118.

Li, Y. G., He, D., Hu, J. M., & Cao, J. (2015). Variability of extreme precipitation over Yunnan Province, China 1960–2012. *International Journal of Climatology, 35*(2), 245–258.

Liu, X., Xu, G., Grießinger, J., An, W., Wang, W., Zeng, X., et al. (2014). A shift in cloud cover over the southeastern Tibetan Plateau since 1600: Evidence from regional tree-ring δ^{18}O and its linkages to tropical oceans. *Quaternary Science Reviews, 88,* 55–68.

Nesje, A. (2005). Briksdalsbreen in western Norway: AD 1900–2004 frontal fluctuations as a combined effect of variations in winter precipitation and summer temperature. *The Holocene, 15*(8), 1245–1252.

Pratap, B., Dobhal, D. P., Bhambri, R., Mehta, M., & Tewari, V. C. (2016). Four decades of glacier mass balance observations in the Indian Himalaya. *Regional Environmental Change*, *16*(3), 643–658.

Prokoph, A., Adamowski, J., & Adamowski, K. (2012). Influence of the 11 year solar cycle on annual streamflow maxima in Southern Canada. *Journal of Hydrology, 442,* 55–62.

Rayner, N. A., Parker, D. E., Horton, E. B., Folland, C. K., Alexander, L. V., Rowell, D. P., et al. (2003). A global analyses of sea surface temperature, sea ice, and night marine air temperature since the late nineteenth century. *Journal of Geophysical Research, 108,* D14. https://doi.org/10.1029/2002JD002670.

Roy, I., & Haigh, J. D. (2010). Solar cycle signals in sea level pressure and sea surface temperature. *Atmospheric Chemistry and Physics, 10,* 3147–3153.

Seko, K., & Takahashi, S. (1991). Characteristics of winter precipitation and its effect on glaciers in the Nepal Himalaya. *Bulletin of Glacier Research, 9,* 9–16.

Shi, Y. F. (2002). Characteristics of late Quaternary monsoonal glaciation on the Tibetan Plateau and in East Asia. *Quaternary International, 97–98,* 79–81.

Torrence, C., & Compo, G. P. (1998). A practical guide to wavelet analysis. *Bulletin of the American Meteorological Society*, *79*, 61–78.

Vinke, K., Martin, M. A., Adams, S., Baarsch, F., Bondeau, A., Coumou, D., et al. (2017). Climatic risks and impacts in South Asia: extremes of water scarcity and excess. *Regional Environmental Change*, *17*(6), 1569–1583.

Wigley, T. M. L., Briffa, K. R., & Jones, P. D. (1984). On the average value of correlated time series, with applications in dendroclimatology and hydrometeorology. *Journal of Climate and Applied Meteorology, 23,* 201–213.

Xu, Z. X., Gong, T. L., & Li, J. Y. (2008). Decadal trend of climate in the Tibetan Plateau—Regional temperature and precipitation. *Hydrological Processes, 22*(16), 3056–3065.

Yang, W., Guo, X., Yao, T., Zhu, M., & Wang, Y. (2016). Recent accelerating mass loss of southeast Tibetan glaciers and the relationship with changes in macroscale atmospheric circulations. *Climate Dynamics, 47*(3), 805–815.

Yao, T., Wang, Y., Liu, S., Pu, J., Shen, Y., & Lu, A. (2004). Recent glacial retreat in High Asia in China and its impact on water resource in Northwest China. *Science in China, Series D: Earth Sciences, 47*(12), 1065–1075.

Zanchettin, D., Rubino, A., Traverso, P., & Tomasino, M. (2008). Impact of variations in solar activity on hydrological decadal patterns in northern Italy. *Journal of Geophysical Research: Atmospheres, 113,* D12102. https://doi.org/10.1029/2007JD009157.

Zhang, Q.-B., Evans, M. N., & Lyu, L. (2015). Moisture dipole over the Tibetan Plateau during the past five and a half centuries. *Nature Communications, 6,* 8062. https://doi.org/10.1038/ncomms9062.

Zhang, R., Sumi, A., & Kimoto, M. (1999). A diagnostic study of the impact of El Niño on the precipitation in China. *Advances in Atmospheric Sciences, 16,* 229–241.

Zheng, B. X., Zhao, X. T., Li, T. S., & Wang, C. Y. (1999). Features and fluctuation of the Melang glacier in the Mainri Mountain. *Journal of Glaciology and Geocryology, 21,* 145–150.

(Received May 2, 2017, revised December 14, 2017, accepted January 11, 2018, Published online January 22, 2018)